Journal of Magnetic Resonance **151,** 269–283 (2001)
doi:10.1006/jmre.2001.2364, available online at http://www.idealibrary.com on IDEAL®

Improved Broadband Inversion Performance for NMR in Liquids

Mari A. Smith, Haitao Hu,[1] and A. J. Shaka[2]

Chemistry Department, University of California—Irvine, Irvine, California 92697-2025

E-mail: ajshaka@uci.edu

Received December 3, 2000; revised April 20, 2001; published online July 3, 2001

New NMR broadband inversion pulses that compensate both for resonance offset and radiofrequency (RF) inhomogeneity are described. The approach described is a straightforward computer optimization of an initial digitized waveform generated from either a constant-amplitude frequency sweep or from an existing composite inversion pulse. Problems with convergence to local minima are alleviated by the way the optimization is carried out. For a given duration and maximum allowable RF field strength B_1 (but not necessarily given RMS power deposition), the resultant broadband inversion pulse (BIP) shows superior inversion compared to inversion pulses obtained from previous methods, including adiabatic inversion pulses. Any existing BIP can be systematically elaborated to build up longer inversion pulses that perform over larger and larger bandwidths. The resulting pulse need not be adiabatic throughout its duration or across the entire operational bandwidth.

Key Words: **two-level system; broadband inversion pulse; population inversion; frequency modulation; adiabatic; high-field NMR; composite pulse.**

INTRODUCTION

The design of a "perfect" 180° pulse to invert longitudinal spin magnetization has been the subject of active research now for two decades (*1–12*). A conventional 180° pulse has very limited tolerance to radiofrequency (RF) field inhomogeneity (or pulse length miscalibration) and provides acceptable inversion only over a relatively narrow resonance offset bandwidth (95% inversion over $\pm 0.2 B_1$). For an RF field strength of 20 kHz, this bandwidth reduces to 4 kHz and is insufficient, for example, to cover the 5-kHz proton range (10 ppm) of a 500-MHz spectrometer. At higher magnetic fields and/or for different nuclei, the chemical shift range is larger and the inadequacies in inversion bandwidth are ever more apparent. Inversion pulses that compensate for either frequency offset, or RF power misset, or both, are thus valuable. "Composite pulses" proposed by Levitt and Freeman (*1*), inversion pulses like the "123" pulse used for WALTZ decoupling (*2, 3*), and adiabatic pulses pioneered by Baum *et al.* (*4*) have all been used with success.

For adiabatic pulses, elegant analytical relationships between the frequency and amplitude modulation have been derived, by examining magnetization trajectories in a suitable reference frame, so that a constant-amplitude pulse implies a tangent function for the frequency sweep (*7*). Likewise, a sech/tanh (amplitude/frequency) combination is commonplace (*4, 6, 7*). The appeal of an adiabatic pulse is that it can achieve a wide band of inversion with moderate RF power and is quite tolerant to inhomogeneties in B_0 and B_1 when the pulse is set at or above the minimum B_1 level determined by the adiabatic condition. This condition requires that the sweep rate is sufficiently slow for the magnetization to remain mostly aligned with the effective field ($\mathbf{B}_{\text{eff}}$). Promising adiabatic inversion pulses have been the sech/tanh pulses (*4, 6, 7*), the WURST family proposed by Kupče and Freeman (*9*), and those produced from the pairing of the hyperbolic tangent and tangent functions suggested by Hwang *et al.* (*12*), the tanh/tan pulses. We have found, however, that big performance gains have gone unrealized by these analytical forms, particularly when a rather short, high-power broadband inversion pulse is desired. This is at least partly because the most useful solution (i) may *not* be entirely adiabatic, and (ii) may be difficult to encapsulate in a simple formula. That is our focus here: the design of a short, broadband (typically) high-power inversion pulse, rather than repetitively applied pulses for decoupling.

Our design focus is on modern high-field experiments in liquids, using well-engineered probes. For most experiments in high-resolution NMR, it is safe to assume that pulses can be approximately calibrated. The intrinsic RF inhomogeneity over the sample volume is not more than ±10%, or ±20% at the outside, i.e., $0.8 < B_1/B_1^0 < 1.2$, with B_1^0 the "nominal" field that would be determined by on-resonance calibration of the 180° pulse width. It is also safe to assume that some maximum B_1 field can be applied without any pulse droop, if the pulse is reasonably short, and that total energy deposition over a short pulse is not an issue. Under these conditions, the hunt for a good inversion pulse reduces to specifying (i) the maximum pulse width, T_p to be used; (ii) the maximum B_1 field, $B_1^{\max}$, that can be employed; and

[1] Current Address: Department of Biochemistry, 896 MRB II, Vanderbilt University, Nashville, TN 37232-0146.

[2] To whom correspondence may be addressed.

1090-7807/01 $35.00

(iii) the exact normalized offset range $\Delta B/B_1^0$ and normalized inhomogeneity range B_1/B_1^0 over which the pulse is to perform. Our measure of the pulse length is the usual one for composite pulses, i.e., in terms of the product $\gamma B_1^{\max} T_p$, which we express in degrees. A conventional inversion pulse has duration "180°" while a 90°_y–180°_x–90°_y composite pulse has duration 360°. This way of measuring the equivalent pulse length is very telling when long delays of low amplitude are included, as in the sech/tanh pulses, which may result in many thousands of degrees in equivalent duration. Some benchmark of the acceptable quality is needed, but 95% inversion or better ($M_z/M_0 = -0.95$) is usually fine. All else being equal, a shorter pulse is to be preferred. For aesthetic reasons, we restrict the pulse to be symmetric in time about its midpoint. This guarantees that the inversion profile has symmetry and halves the number of points over which the performance must be calculated. For simplicity, and because the pulses are always assumed to be short in duration, relaxation is neglected.

It is within this framework that we set out to investigate the limits of broadband inversion. We found that it is unnecessary to shape the amplitude of the waveform, which is a slight surprise when weighing arguments revolving around adiabaticity (*9–12*). There is also a collateral benefit to a constant-amplitude pulse: by keeping the amplitude constant throughout, the linearity of the RF amplifier is not as important as it would be for amplitude-modulated pulses. This is a consideration when high-power pulses must be used, as then some pulse compression is usually inevitable, implying nonlinearity of the RF amplifier. Finally, strictly speaking, a rectangular phase-modulated pulse does not necessitate a waveform generator, as the digital frequency synthesizer is fully capable of producing the requisite phase shifts. This may be a factor on older instruments or on spectrometer consoles incompatible with newer waveform circuit boards.

THEORY

In principle a pulse waveform can be specified in terms of either frequency modulation (FM) or phase modulation (PM). In practice, the spectrometer hardware accepts shapes as a list of events, each specifying an amplitude and *phase* pair for specified duration. Thus, ultimately, phase modulation is preferred. Frequency modulation is useful, however, because a pulse derived from an FM waveform is intrinsically smoother. This is easy to understand because phase is the integral of frequency, so that a continuous shape in frequency always integrates to a smoother shape in phase. Conceptually, the FM picture fits well with the adiabatic view that the magnetization vector **M** should follow the effective field in the FM frame (*7*). The decided disadvantage of using the FM description is that instantaneous phase shifts, for example, those present in the 90°_y–180°_x–90°_y composite pulse, are difficult to represent because the phase profile is *not* smooth. In practice we may use both descriptions at various points in the pulse waveform optimization, depending on which representation is most useful. In the end, a purely digital PM waveform is produced as a list of phases: there is no underlying functional form. However, the phase list may be fitted *post hoc* to any convenient functional form so that pulses of different lengths can be digitized in exact registration with the spectrometer waveform hardware timing resolution.

The design of our inversion waveform, being unconstrained by any analytical functional form or prespecified trajectory, has its initial form generated either from a linear frequency sweep or, for very short pulses, from a 90°_y–180°_x–90°_y composite pulse template. The amplitude and duration of the pulse over a given optimization run are both fixed. This initial guess at the phase modulation is then numerically optimized, to create a family of rectangular phase-modulated pulses with dual compensation, which we refer to as *b*roadband *i*nversion *p*ulses (BIPs). Compared to sech or tanh pulses, the new BIPs give superior inversion performance for a given duration and peak RF power. In addition, these pulses can be tailored, by varying the pulse width and peak power, to accommodate different nuclei of interest.

Exact Integration of a Phase-Modulated Pulse

It is a simple matter to solve the von Neumann equation for the reduced density operator σ

$$\dot{\sigma} = -i[\mathcal{H}, \sigma] \qquad [1]$$

exactly for an ensemble of isolated spins and finite number of time-independent states using rotation operators. During each state k of the waveform the Hamiltonian $\mathcal{H}_k$ can be written in the form

$$\tau_k \mathcal{H}_k = \beta_k \mathbf{n}_k \cdot \mathbf{I}, \qquad [2]$$

where β_k is an angular variable and $\mathbf{n}_k$ is a unit vector, and the reduced density operator $\sigma_k = \mathbf{m}_k \cdot \mathbf{I}$ is transformed into

$$\sigma_{k+1} = \mathbf{m}_k \cdot \mathbf{I} \cos\beta_k + (\mathbf{n}_k \cdot \mathbf{m}_k)(\mathbf{n}_k \cdot \mathbf{I})(1 - \cos\beta_k) + (\mathbf{n}_k \times \mathbf{m}_k) \cdot \mathbf{I} \sin\beta_k \qquad [3]$$

from which the normalized inversion after N steps can be calculated:

$$\langle I_z \rangle_0 = \frac{Tr\{I_z \sigma_N\}}{Tr\{I_z^2\}}. \qquad [4]$$

This calculation can then be repeated over the offset range $\Delta B/B_1^0$ and misset range B_1/B_1^0 over which the pulse is to perform.

Optimization of a PM Waveform

As the performance of a given waveform can be calculated exactly, optimization of the most general shape is then a straightforward nonlinear least-squares problem with the objective

function

$$S(\Omega, \Phi) = \sum_{\Delta B/B_1^0} \sum_{B_1/B_1^0} (\langle I_z(\Omega, \Phi)\rangle_0 + 1)^2 \qquad [5]$$

and with the amplitude $\omega_k = \gamma B_{1k}$ and phase φ_k of each event as a variable. The summation is carried out over a rectangular grid of points in offset and RF field strength. A typical pulse waveform could have hundreds of events, with the phase specified to better than 1°, and the relative amplitude to 1 part in 1000. A straightforward grid search, as has been attempted in other contexts (*13*), of a 500-point waveform would, for example, require $\sim 360^{500} 1000^{500} = 10^{2778}$ integrations of the waveform over the grid of offset and B_1 values. If the nominal amplitude B_1^0 is also allowed to vary, matters get even worse. Clearly it is not possible to conduct any type of brute-force event-by-event search to determine the best waveform. One might be tempted to try a simulated annealing algorithm (*14*) as has been used with success to optimize purely amplitude-modulated selective pulses like I-BURP (*15, 16*). However, even simulated annealing is unlikely to yield anything useful unless a representative fraction of the available parameter space can be sampled, and even with millions of trials this will not be the case for the present problem.

These major difficulties are one reason why some relatively simple functional form is usually assumed up front, with a *small* number of parameters to optimize. The art is then to choose the right form. Even when the form is made as general as a Fourier series (*16*) the essential point is that only a controllable number of Fourier coefficients need enter into the optimization because amplitude shapes of interest can be represented with only a few terms. By contrast, typical phase profiles are definitely *not* conveniently expressible as a small number of sinusoids: a linear frequency sweep leads to a parabolic phase profile, a case in the which the Fourier series is not uniformly convergent. Even with the amplitude and pulsewidth fixed, however, the phase space is far too large to search directly.

One possibility is to express the phase function as an even-order polynomial, e.g.,

$$\varphi(t) = \sum_n \Phi_n t^{2n} \qquad [6]$$

for a pulse defined over the time interval $-T_p/2 < t < T_p/2$, and then optimize the coefficients Φ_n up to some maximum value $n = K$. While initially attractive, this formulation is plagued by many, many local minima that are widely spaced in the parameter space, and the highest power $2K$ is hard to pin down. For example, a Taylor series expansion of $\tan x$ (suggested as an appropriate FM for a long constant-amplitude pulse (*7*)) leads to terms with ever-growing coefficients that always approximate the function poorly at the edges ($x = \pm\pi/2$) when a finite number of terms are used. Finally, as noted above, most simple composite pulses have discontinuous phase jumps that cannot be well approximated by Eq. [6].

Accepting that the most general possible PM pulse is simply a list of phases, and that the parameter space for a long waveform is huge, even with the amplitude function held constant, the most important factor is to locate a decent starting point. Fortunately, there are plenty of existing possibilities. Then we can try to use an optimization strategy that somehow limits the possibilities without actually presupposing any particular functional form, and without sampling even a small fraction of the totality of parameter space. The main optimization weapon we have used is to suppose that the final PM should be "smooth enough" in the sense that averaging a small enough number of adjacent events should produce a waveform that does not degrade the performance much.

The search is conducted in three different modes, depending on the nature of the starting waveform and the progress being made. From a composite pulse with discontinuous phase shifts, the approach is to progressively subdivide each time segment until the performance does not substantially improve. For example, the composite pulse 90°_y–180°_x–90°_y can be divided into four equal time steps, e.g., 90°_y–90°_x–90°_x–90°_y, and has two phase events as free parameters when taking account of the symmetry. Fixing the central pulse to phase $+x(0^\circ)$, there is just one phase to optimize. By dividing each pulse into two, an 8-step pulse with three free parameters is created. This waveform is then optimized. The process of subdivision and optimization is continued until a 360° length composite inversion pulse with (possibly) a fairly smooth waveform is produced. This sequence of optimizations is far more effective than attempting to create a finely divided pulse in a single step.

If the starting waveform is *already* smooth, for example, the quadratic phase profile obtained from a linear frequency sweep, then the pulse can be digitized to the final desired resolution right away. We simply choose the smallest value for the discrete number of events that does not degrade the computed performance appreciably. In this case the second strategy is used: small phase ramps are added at random about a randomly chosen "pivot" in the waveform, as shown in Fig. 1. This corresponds to shifting, slightly, the frequency at a certain point in time, and is effective in shaping the phase and keeping it sensibly smooth, without presupposing any functional form. This second strategy gives a quick coarse optimization into a nearby local minimum.

The final step is to treat each phase itself as a variable, and randomly perturb it to see if the performance of the pulse can be improved. A strictly downhill Monte Carlo search, in which the phase of each event φ_k on the nth trial is randomly perturbed, e.g.,

$$\varphi_k^{(n+1)} = \varphi_k^{(n)} + \varepsilon_k \qquad [7]$$

(and the new waveform is accepted only if the performance is better) is completely general but would suffer from problems with local minima and potentially generate very "rough" modulation. To bias the search toward the direction of smoother shapes it is sufficient to replace, from time to time, a percentage of such

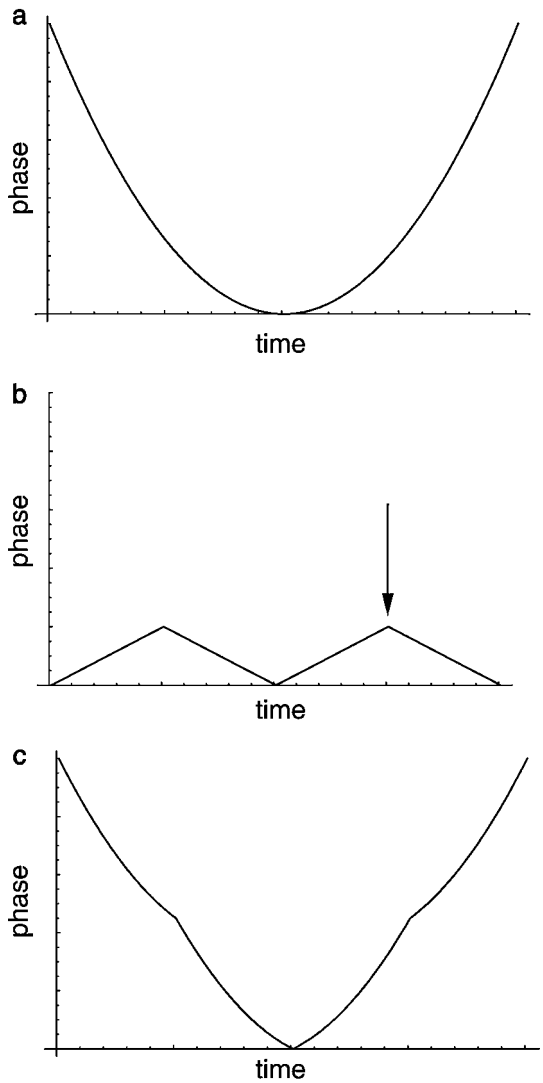

FIG. 1. A generic way to perturb a phase function, keeping it continuous. The smooth shape in (a) has the perturbation in (b) (which has been exaggerated for clarity) added to it, to give (c), a new trial phase function. The function in (c) is accepted if it gives superior performance, and the process is repeated many times. The "pivot point" in (b), set out with an arrow, is chosen at random, as is the magnitude and sign of the phase perturbation applied at this point, and at the end of the pulse. The other half of the phase function is obtained by symmetry. A linear phase ramp corresponds to a slight frequency shift of the pulse, and is an effective, physically motivated, optimization tool.

a smoothed waveform for an equal percentage of the current shape:

$$\Phi \rightarrow (1-\delta)\Phi + \delta\Phi_s, \qquad [8]$$

where $0 < \delta < 1$ is a small number and Φ_s is a smoother phase profile. This is a kind of "superannealing" step that, in general, degrades the performance-sometimes greatly, but, in the long run, the only shapes that can emerge are those that have performance that is *not* drastically degraded by this smoothing, i.e., waveforms that are themselves sufficiently smooth. Our Monte Carlo algorithm is thus strictly downhill optimization, with a small fraction of unconditional moves based on Eq. [8], without regard to how the performance is affected. There is no proof that this algorithm locates the global minimum, or that it in fact converges to anything at all, so its worth will be judged by the performance of the pulses produced. Used intelligently, we have found that the smoothing criterion sidesteps the myriad local minima that would arise from purely random phase jumps, without sampling irrelevant regions of parameter space like the simulated annealing method tends to do. Its basis is clearly grounded in the observation that a pulse with discontinuous phase jumps is not going to be adiabatic, so that "smoother" could be expected, on average, to be "better." The longer the pulse is, the more likely that an adiabatic solution will be good, and this is exactly the case when the number of parameters and local minima get huge. We mostly employed a simple $1:2:1$ convolution of three adjacent events to smooth the waveform and obtain Φ_s, although this choice is fairly arbitrary, and the results do not depend sensitively on it.

Partially Adiabatic Pulses

The adiabatic condition (*17*) dictates that the magnetization $\mathbf{M}$ and the effective field $\mathbf{B}_{\text{eff}}$ remain rather closely aligned throughout the trajectory (*7*), which in turn sets a minimum duration for an adiabatic pulse. A conventional 180° pulse is only just long enough to invert spins on resonance, and with $\mathbf{M}\cdot\mathbf{B}_{\text{eff}} = 0$ throughout the trajectory, is clearly not adiabatic on resonance. Rather more interesting are simple composite pulses like 90°_y–180°_x–90°_y, for which the on-resonance trajectory is adiabatic during the central 50% of the pulse, but nonadiabatic elsewhere. We could thus view this first composite pulse as a very poorly digitized continuous PM pulse that has an adiabatic portion near resonance, and so shows some compensation for RF field inhomogeneity near resonance. Clearly, partially adiabatic pulses may be important in the quest for a short, compact PM pulse. This observation motivated the subdivision strategy, starting with this initial condition.

There is a hidden difficulty when the length of the starting pulse is not matched well to the desired bandwidth, for example, using a 90°_y–180°_x–90°_y starting point and attempting to invert well over the range $\Delta B/B_1^0 = \pm 0.5$ and $B_1/B_1^0 = 1 \pm 0.2$. After much frustration, one is forced to conclude that *no such pulse exists*; that is, there is a minimum duration required to achieve good inversion performance over this range, and that it must be longer than 360°. Because the algorithm described above never alters the length of the pulse, no acceptable solution will ever be found. The way this is handled is to fix the $B_1/B_1^0 = 1 \pm 0.2$ range and then locate the maximum offset range $\Delta B/B_1^0$ over which inversion *is* acceptable, following the recipe above. This pulse is then fixed, and additional phase events are added symmetrically on either end, using (i) simple extrapolation of the phase or (ii) a linear phase ramp

corresponding to an off-resonance pulse well outside the currently optimized bandwidth. Only the new phase events are optimized initially, the entire central portion being calculated as a single rotation operator. Once no further improvement is obtained using this edge optimization, then progressively more and more of the entire pulse is subjected to optimization, working in from the edges and finishing with the whole pulse.

The basis for this sequential optimization is that the initial and final portions of the pulse are essentially far off resonance, and have little effect on the previously optimized inversion band. That is, they amount to near *z* rotations over most of the interior offset range and so cannot affect the inversion performance much there. It makes sense that their role is therefore to influence the performance at the edges of the bandwidth, so that there is little point in reoptimizing any of the phases in the central portion of the waveform until the edges have stabilized. This great simplification lets very long pulses be built up quickly and systematically. It also allows us to get a feel for exactly what is possible. A similar strategy of employing *z* rotations to create inversion pulses from decoupling expansions (*18*) gave some useful results for phase-alternating 180° pulses (*8*). Those strategies fail in the current context because the inversion bandwidth rapidly exceeds the bandwidth of a 90° pulse, the main weapon in the decoupling expansion strategy (*18*). Phase-alternating inversion pulses also show little tolerance for RF inhomogeneity near resonance, less uniform performance, and smaller bandwidths for a given duration than the BIPs we present here.

NUMERICAL RESULTS

Figure 2 shows the effect of the smoothing steps on the final optimized waveform. A 90°_y–180°_x–90°_y pulse was digitized into 500 events and optimized by downhill Monte Carlo without (a) and with (b) the smoothing steps. The jagged waveform in 2a apparently became trapped in a local minimum and failed to improve after thousands of trials—although the performance was quite good. By contrast, the periodic smoothing steps resulted in an appealing, smooth phase function that converged rapidly and that delivers marginally better performance, as shown in the lower traces 2c–2e. While simulated annealing should, in principle, be able to convert 2a mindlessly into 2b, the amount of CPU time required would be formidable. Note that 2b was obtained *without* using the subdivision strategy. Using the latter, in conjunction with smoothing, results in 2b reproducibly and almost instantaneously. This does not prove that 2b is the global minimum, of course, but it does show that our approach gives good performance quickly, and that the solution is insensitive to the exact way the optimization is carried out. Figure 3 shows a sampling of some of the digital phase functions for the sequence of pulses obtained, beginning with the 90°_y–180°_x–90°_y pulse and using successive subdivision and optimization. The sequence clearly converges to the nonlinear frequency sweep of 2b, *one that reverses sense at the edges of the pulse*. This behavior is shown in Fig. 4, in which the phase and frequency profiles are

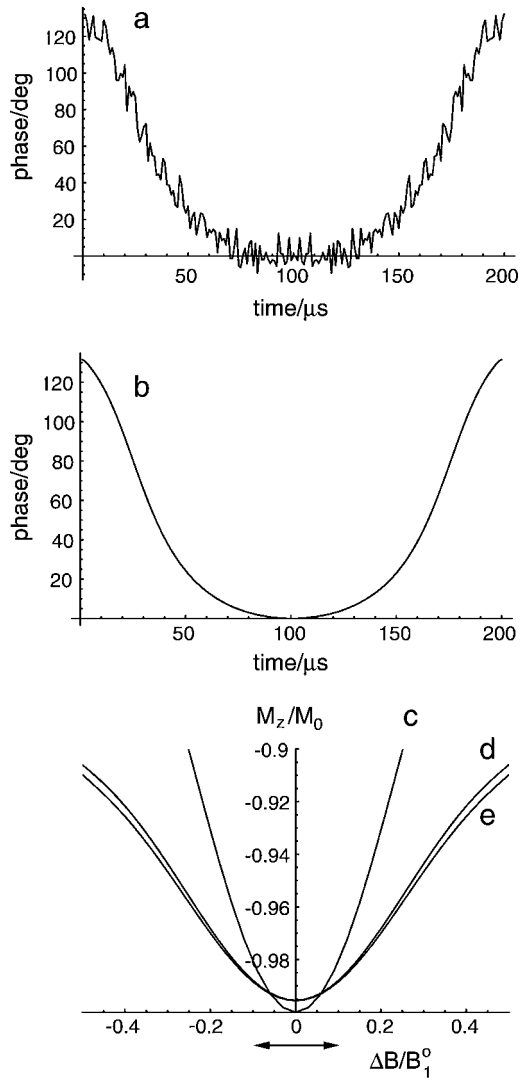

FIG. 2. Phase profiles resulting from optimization of a 500-point digitized 90°_y–180°_x–90°_y composite pulse, perturbing each phase variable independently. In (a) downhill Monte Carlo optimization was used, leading to a jagged phase modulation. In (b) a number of smoothing steps were incorporated, as described in the text. The dominant low-frequency components in (a) emerge, without the jagged noisy excursions. The calculated inversion profiles of the original composite pulse (c), the jagged pulse (d), and its smooth cousin (e) are shown in the bottom panel. The offset optimization range was ± 0.1, as indicated by the horizontal double-headed arrow. The inhomogeneity optimization range was $B_1/B_1^0 = 1 \pm 0.2$. Inversion as a function of offset is plotted at the nominal setting, B_1^0.

shown together. This kind of "sweep" is in contrast to the modulated inversion pulses (MIPs) of Baum *et al.* (*7*), in which the frequency sweep accelerates away rapidly at the pulse edges. The numerical approach gives the somewhat unexpected result that the sweep should revert backward on itself at the edges, at least for pulses of this length optimized over this bandwidth. As the BIP frequency profiles are invariably rather complex, and offer little insight into the mechanism of action, we will not plot further frequency profiles to economize on space.

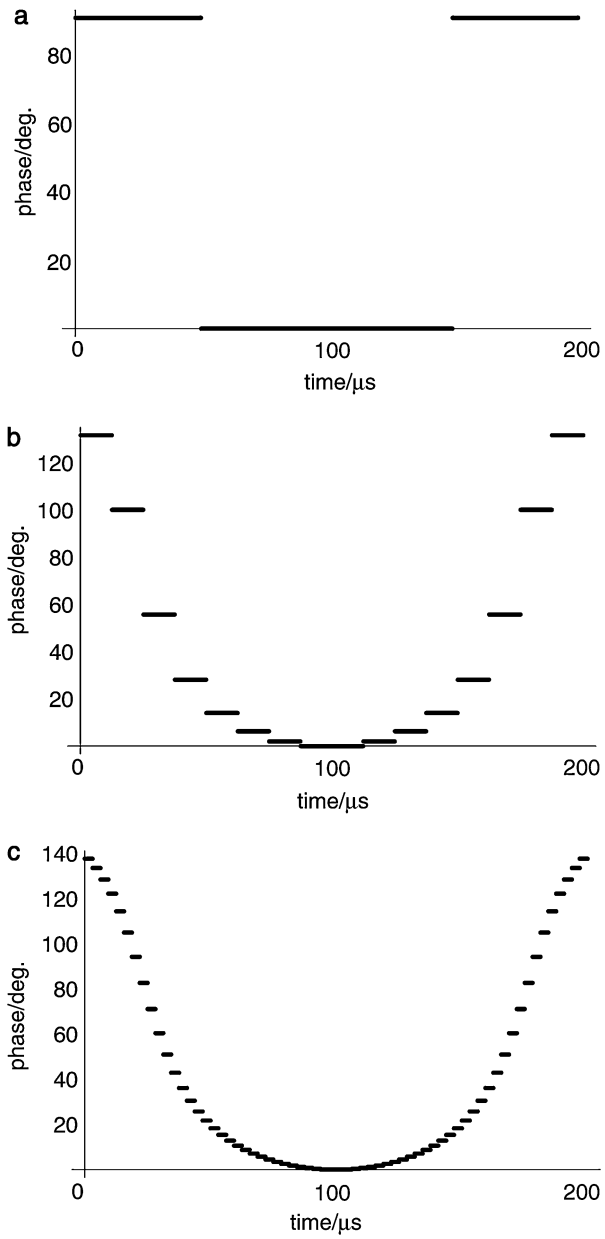

FIG. 3. Evolution of a smooth phase-modulated pulse from a simple composite pulse. Successive subdivision and optimization led to the profiles shown in (b) and (c). Including more and more events leads to the smooth function shown in Fig. 2b. The timing on the abscissa is appropriate for an RF field of 5 kHz.

A smooth functional form should be fairly easy to fit as a power series, and doing so to the smooth shape in Fig. 2b shows why the form of Eq. [6] is tricky to work with. Letting

$$\tau = \frac{t}{\left(\frac{T_p}{2}\right)}, \quad |\tau| < 1 \qquad [9]$$

be the normalized time variable for the pulse of length T_p the phase function for 2b is, approximately,

$$\frac{\varphi(\tau)}{\text{deg.}} = 33.0986\tau^2 + 301.112\tau^4 - 201.959\tau^6, \qquad [10]$$

showing a very strong deviation from a linear sweep (which would be a purely quadratic phase function), and a negative coefficient that bears no relationship to those predicted from the ln(cos(x)) series derived from a tangential frequency sweep (*7*). The presence of large terms that partially cancel each other makes finding Eq. [10] from Eq. [6] a difficult problem for conventional optimization strategies, particularly when the appropriate number of terms to include in the power series is not known beforehand.

Figure 5 shows a comparison that illustrates the flexibility of dual compensation that can be achieved. The first three panels are BIPs of length 720°, optimized over the rectangular regions indicated. The final panel is the GROPE-16 composite pulse (*19*) that mimics a 90°_y–180°_x–90°_y pulse with the inclusion of some approximate "inverse" pulses (*3*, *5*). Unfortunately, GROPE-16 is of length 1440° and has a fixed range of dual compensation that is not easily adjusted. It is clearly not even remotely competitive with the new generation of BIPs.

By carrying out a large number of successive optimizations over various bandwidths, we have arrived at the summary shown in Table 1. The fit to piecewise cubics is only approximate, but

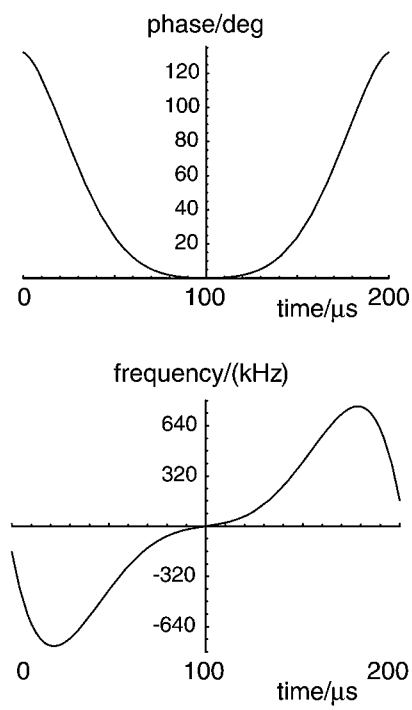

FIG. 4. A comparison of the phase and frequency profiles for the optimized pulse obtained in Fig. 3. The frequency sweep reverses sense at the edges of the pulse, rather than accelerating away, the latter being the expected endpoint if an adiabatic mechanism were operative. The effective field is not oriented near the $\pm z$ axis at either the beginning or the end of the pulse.

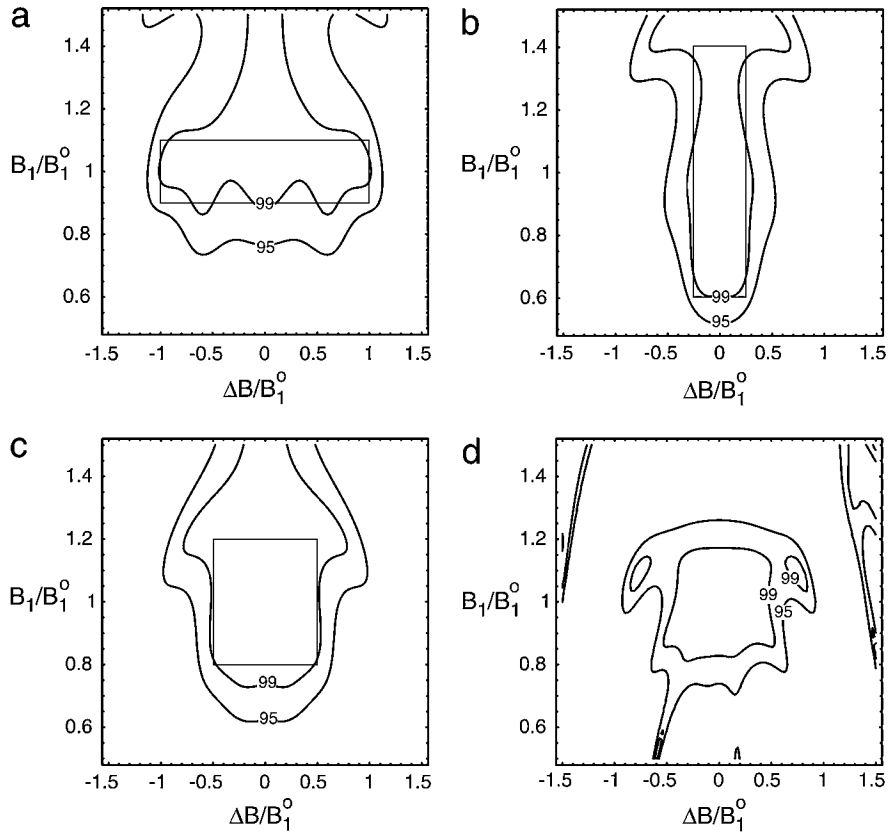

FIG. 5. Three BIPs (a–c) and a GROPE (d). The BIPs have been optimized over the indicated rectangular regions. They have length 720° and are designated as BIP–720–100–10, BIP–720–25–40, and BIP–720–50–20, respectively. The GROPE-16 pulse is of length 1440°, and is not as effective as BIP–720–50–20 even though it is twice the duration of the latter.

adequate for most purposes. The exact phase lists produced by the optimizations themselves, which give slightly better performance, can be obtained from the authors. To simplify the designation of a particular pulse we have adopted the notation BIP–*dd*–*xx*–*yy*, where *dd* is the length of the pulse in degrees, *xx* is the percentage, $xx = \Delta B/B_1^0 \times 100$, of positive offsets over which inversion is good, and *yy* is the percentage $B_1^0[1 \pm (yy/100)]$ of inhomogeneity compensation. Thus, BIP–720–50–20 denotes a broadband inversion pulse of length 720° that inverts well over the offset range $\Delta B/B_1^0 = \pm 0.5$ and $B_1/B_1^0 = 1 \pm 0.2$, etc.

Comparison with Adiabatic Pulses

Clearly, it is possible that numerical optimization might lead straight back to an existing analytical pulse shape or a known adiabatic pulse calculated according to an empirical formula like the WURST pulses of Kupče and Freeman (*9*). The longer the pulse width, in degrees, the more likely that a purely adiabatic solution could emerge as optimum, especially with a built-in bias toward smoother phase modulation. This is apparently not the case, however, as the experimental results of the next section will make clear. From an optimization point of view, adiabatic pulses, which are known to perform better and better as the B_1 field is increased, might arise by choosing a very large range, say $0.8 < B_1/B_1^0 < 5.0$, of inhomogeneity compensation. This is clearly counterproductive when the maximum available field is already being used and when the known upper limit of B_1/B_1^0 on any decent liquids probe is 1.2. Including this irrelevant range in B_1/B_1^0 can only lead to worse offset performance in $\Delta B/B_1^0$, as the contour plots in Fig. 5 clearly illustrate. When the total duration is less than about 720°, there is not enough time for most of the adiabatic pulses to operate at all, but useful solutions are still obtained by our approach.

EXPERIMENTAL

As the motivation to develop the BIPs arose from previous experiments in which they have already been employed (*20, 21*) there is abundant evidence that they perform as calculated. Nevertheless, to compare with other possibly competitive shapes in the literature, and to verify that there is no apparent hardware limitation, simple inversion profiles were obtained on a Varian UnityPlus 500 MHz spectrometer using a Varian triple-resonance probe equipped with a shielded PFG coil. The inversion pulse was followed by a brief pulsed field gradient to disperse any transverse magnetization, the remaining *z*-magnetization being subsequently read out with a conventional

TABLE 1
Representation of BIPs as Piecewise Cubics

τ_{min}	τ_{max}	a_0	a_1	a_2	a_3
			BIP–30–5–360.RF		
0.0000	3.0709	0.00	0.000	0.832	0.03853
3.0709	6.2205	−23.30	20.084	−5.5846	0.55904
6.2205	7.4016	−127.08	191.539	−52.6649	4.12778
7.4016	8.5827	−5998.88	1953.579	−207.2433	7.32952
8.5827	10.0000	−1237.67	389.593	−36.6984	1.15958
			BIP–20–10–360.RF		
0.0000	3.0709	0.00	0.000	0.3704	0.02097
3.0709	6.2205	−16.83	15.474	−4.3532	0.49946
6.2205	7.4016	1171.06	−479.512	62.6958	−2.42231
7.4016	8.5827	2468.83	−1070.420	151.2993	−6.80748
8.5827	10.0000	−684.02	184.608	−12.7523	0.25618
			BIP–5–25–360.RF		
0.0000	3.0709	0.00	0.000	−0.5869	0.21875
3.0709	6.2205	12.28	−8.173	0.8303	0.19999
6.2205	7.4016	24.67	−31.672	7.4247	−0.30432
7.4016	8.5827	−132.12	7.634	5.3899	0.36021
8.5827	10.0000	−554.77	135.553	−7.2060	0.03933
			BIP–75–15–540.RF		
0.0000	1.9840	0.00	0.000	1.4243	−0.03920
1.9840	3.9880	8.43	−8.882	3.9535	−0.13694
3.9880	5.9920	106.09	−73.563	17.9689	−1.12421
5.9920	7.9960	−163.25	82.551	−11.6331	0.71992
7.9960	8.9980	−1973.56	995.187	−154.9630	7.91199
8.9980	9.4990	−3376.91	366.465	36.7830	−3.70610
9.4990	9.7996	−124463.94	38356.720	−3936.1061	134.77807
9.7996	10.0000	−688333.33	208817.376	−21110.3978	711.46585
			BIP–100–10–720.RF		
0.0000	1.9840	0.00	0.000	0.1422	0.87595
1.9840	3.9880	4.90	−9.487	5.9731	−0.28003
3.9880	5.9920	−58.90	35.686	−4.6477	0.54867
5.9920	7.9960	66.68	−29.634	6.6624	−0.10325
7.9960	8.9980	−12316.05	4493.881	−543.7607	22.20473
8.9980	9.4990	−63946.67	21652.640	−2444.5706	92.39319
9.4990	9.7996	199261.17	−64010.045	6840.4442	−242.79843
9.7996	10.0000	159958.18	−50767.812	5365.6444	−188.43240
			BIP–50–20–720.RF		
0.0000	1.9840	0.00	0.000	1.0879	0.23278
1.9840	3.9880	2.09	−2.865	2.3850	0.03950
3.9880	5.9920	22.34	−16.172	5.2386	−0.15860
5.9920	7.9960	−124.32	57.071	−6.9545	0.51800
7.9960	8.9980	−6216.57	2353.392	−295.4618	12.60033
8.9980	9.4990	88298.17	−28318.754	3019.9834	−106.76385
9.4990	9.7996	335738.95	−105999.551	11148.6467	−390.28632
9.7996	10.0000	−31146.49	7862.432	−628.1105	15.66463
			BIP–25–40–720.RF		
0.0000	1.9840	0.00	0.000	2.2960	−0.32494
1.9840	3.9880	8.31	−7.835	3.8594	−0.18678
3.9880	5.9920	−1.38	0.524	1.4951	0.03329
5.9920	7.9960	−66.81	39.030	−5.8899	0.49744
7.9960	8.9980	−1835.27	784.775	−109.4400	5.24295
8.9980	9.4990	23934.76	−7645.390	809.4766	−28.13261
9.4990	9.7996	−133834.07	41587.176	−4310.8679	149.35162
9.7996	10.0000	422611.92	−129850.735	13294.7752	−453.28889
			BIP–75–15–720.RF		
0.0000	1.9840	0.00	0.000	2.2393	0.12622
1.9840	3.9880	11.08	−14.099	8.0081	−0.61827
3.9880	5.9920	−35.81	26.687	−3.6014	0.46765

TABLE 1—*Continued*

τ_{min}	τ_{max}	a_0	a_1	a_2	a_3
5.9920	7.9960	1190.22	−529.823	79.7074	−3.63460
7.9960	8.9980	−9053.38	3321.951	−403.0683	16.53544
8.9980	9.3988	−2669.23	2481.179	−452.7443	23.67746
9.3988	9.6994	180224.27	−59270.107	6476.3165	−234.79515
9.6994	10.0000	92450.55	−29218.390	3078.6586	−107.74230
			BIP–90–15–810.RF		
0.0000	1.9522	0.00	0.000	4.7482	−0.76556
1.9522	3.9442	27.59	−28.955	12.6921	−0.94587
3.9442	5.9363	−1.59	−0.524	3.9041	−0.06965
5.9363	7.9283	531.45	−219.837	32.4139	−1.19691
7.9283	8.7251	−10953.53	3915.096	−462.5280	18.49386
8.7251	9.3227	−84278.79	28978.823	−3318.1537	126.94155
9.3227	9.7211	446429.42	−142281.355	15103.6561	−533.57475
9.7211	10.0000	343281.82	−105524.685	10815.9473	−369.18000
			BIP–125–15–900.RF		
0.0000	1.9840	0.00	0.000	3.0118	0.49239
1.9840	3.9880	8.85	−13.807	10.1821	−0.74779
3.9880	5.9920	−13.89	18.959	−1.9599	0.59524
5.9920	7.9960	−1343.97	601.301	−85.1971	4.44969
7.9960	8.9980	12194.50	−4453.146	543.7961	−21.64103
8.9980	9.2986	46149.93	−14657.871	1553.8492	−54.46298
9.2986	9.5992	−106039.89	38252.123	−4545.8981	178.88367
9.5992	9.7996	−1965320.74	601349.240	−61334.0200	2085.82748
9.7996	10.0000	−1259072.11	379331.238	−38085.2526	1274.85179
			BIP–120–20–900.RF		
0.0000	2.1203	0.00	0.000	5.0897	−0.33385
2.1203	4.2693	7.81	−7.322	6.7860	−0.32432
4.2693	6.4183	290.43	−171.583	37.2188	−2.07252
6.4183	7.8510	−594.01	310.760	−48.6739	2.94616
7.8510	8.5673	6379.75	−2467.543	319.6628	−13.30632
8.5673	9.1404	−17454.72	5964.158	−674.5029	25.76312
9.1404	9.3410	−554474.55	181639.005	−19830.4143	722.02080
9.3410	9.5702	297190.60	−89281.416	8894.1329	−293.06427
9.5702	9.7708	−2763100.69	850137.095	−87187.2561	2981.05664
9.7708	10.0000	−865607.64	260978.268	−26218.1896	878.18462
			BIP–250–15–1382.RF		
0.0000	2.5654	0.00	0.000	12.3388	−0.37360
2.5654	5.1832	9.68	−6.109	12.6895	−0.15535
5.1832	7.8010	65.09	−25.300	13.9075	−0.07389
7.8010	8.8482	−2126.58	812.761	−92.9098	4.46419
8.8482	9.3717	−12358.11	4472.530	−528.0852	21.67046
9.3717	10.0000	−83165.75	27391.088	−3000.4957	110.56624

Note. $\varphi(^\circ) = a_0 + a_1|\tau| + a_2|\tau|^2 + a_3|\tau|^3; -10 \le \tau \le 10.$

90° pulse. The test sample was the ASTM standard "2-Hz" H_20/D_20 sample, doped with 0.1 mg/ml $GdCl_3$. The RF power was carefully calibrated and set at 20 kHz. The resonance offset of the inversion pulse was incremented in 1-kHz steps over the range indicated in the accompanying figures. The 90° read pulse was applied on resonance. The pulses were usually digitized in 250-ns increments, although 0.5-μs increments gave essentially identical profiles.

Experimental Inversion Profiles

Figure 6 shows the experimental inversion profiles of a conventional hard 180° pulse, two sech/tanh (amplitude/frequency) pulses with different sweep bandwidths, an optimized tanh/tan (amplitude/frequency) pulse, and one of our BIPs, using an offset range of ±50 kHz and an RF field $\gamma B_1/2\pi = 20$ kHz. A pulse length of 192 μs was employed for all pulses except the hard 180° pulse, which of course required a 25-μs pulse length. The equivalent length of the other pulses was thus 1382.4°, slightly shy of four 360° rotations.

The sech pulse amplitude profile was computed from the function

$$B_1(t) = B_1^{\max} \operatorname{sech}\left(\frac{2\beta t}{T_p}\right), \qquad [11]$$

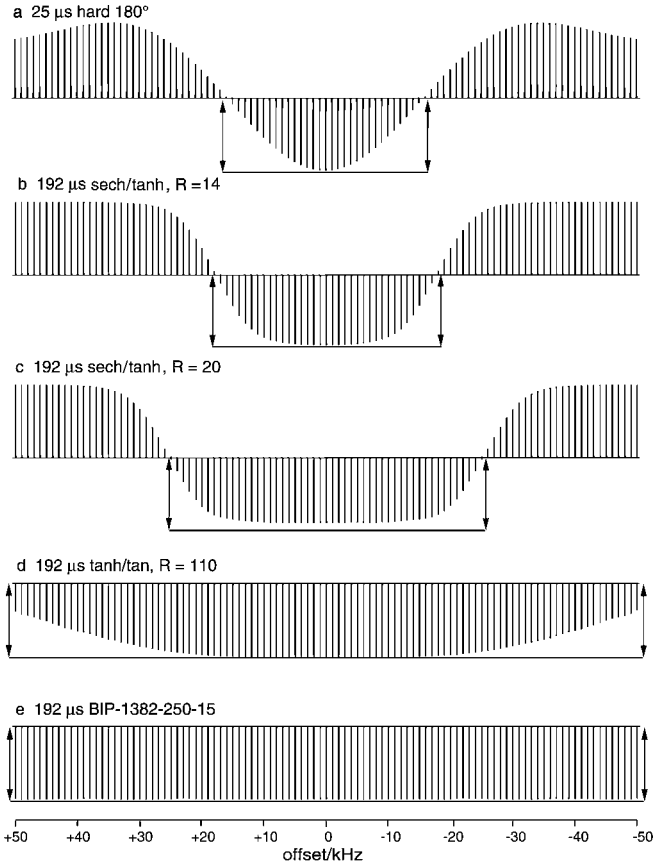

FIG. 6. Experimental inversion profiles of a series of 192-μs pulses at a 20-kHz maximum RF field. (a) The performance of a conventional 180° pulse, of length 25 μs. (b) A sech/tanh pulse, truncated at 1% amplitude, with $R = 14$, showing uniform inversion over a wide band. (c) The same pulse in (b) but with a faster sweep rate, corresponding to $R = 20$. Offset performance is improved only with degradation of the percentage inversion over the band. (d) The tanh / tan pulse described in the text, showing an even larger range of good inversion than the sech pulses. (e) The BIP–1382–250–15 pulse, dwarfing the adiabatic pulses. Inversion is essentially perfect over ±50 kHz. The horizontal lines are meant to guide the eye, delineating 100% inversion.

while the phase was calculated from the function

$$\varphi(t) = \varphi_0 \ln\left\{\frac{\cosh(\beta)}{\cosh\left(\frac{2\beta t}{T_p}\right)}\right\}, \qquad [12]$$

where $\mathrm{sech}[\beta] = 0.01$, $B_1^{\max}$ is peak RF field, $\varphi_0 = \frac{R\pi}{2\beta}$, $R =$ bandwidth* T_p, T_p is the pulse length, and $-T_p/2 \le t \le T_p/2$ (*4, 12*). The parameter β was fixed at 5.3, giving 1% truncation at the edges of the pulse. The parameter R was varied and it was noted that $R = 14$ gave the best inversion while values greater than 14 increased the offset bandwidth but decreased the inversion performance; R values less than 14 decreased both the offset bandwidth and the inversion. Two representative inversion profiles of the sech/tanh pulses, with $R = 14$ and $R = 20$, were obtained experimentally and are shown in Figs. 6b and 6c, respectively. It is obvious that the bandwidth is improved as R is increased from 14 to 20 but the extent of inversion is compromised. Although Tannus and Garwood (*11*) proposed raising the sech pulse to some power to account for the peak power limitations of the standard sech/tanh pulse, a different family of pulses (tanh/tan) that exhibited better inversion performance with respect to offset was subsequently introduced (*12*). The minor difference between these pulses and MIP pulses of Baum *et al.* (*7*) is only the slightly rounded edges of the tanh amplitude profile of the former compared to the constant amplitude of the latter.

The tanh/tan pulse amplitude was calculated, from the formula

$$B_1(t) = B_1^{\max} \tanh\left[\xi\left(1 - \left|\frac{2t}{T_p}\right|\right)\right], \qquad [13]$$

where $\xi = 10$, $B_1^{\max}$ is the maximum RF field, T_p is the pulse length, and $-T_p/2 \le t \le T_p/2$. The phase function was derived from the generic function

$$\varphi(t) = \varphi_{\max} - \frac{AT_p}{2\kappa \tan[\kappa]} \ln\left\{\frac{\cos\left(\frac{2\kappa t}{T_p}\right)}{\cos[\kappa]}\right\} \qquad [14]$$

with the particular values

$$\tan\kappa = 20 \qquad [15]$$

$$\varphi_{\max} = -\frac{AT_p}{2\kappa \tan\kappa} \ln(\cos(\kappa)) \qquad [16]$$

$$A = \frac{R\pi}{T_p} \qquad [17]$$

and with $R = 110$, as described by Hwang *et al.* (*12*). Once again the phase equations depict only half of the waveform, the other half being calculated by symmetry. Figure 6d is the experimental inversion profile of the tanh/tan pulse. While the inversion bandwidth is increased compared to those generated from the sech pulses, complete inversion begins to fail before an offset of ±20 kHz.

Figure 6e shows the inversion profile of our numerically optimized BIP–1382–250–15. This pulse was optimized for a ±50-kHz offset and a ±15% RF field tolerance, using 384 points, or 0.5 μs resolution. It displays nearly ideal inversion across the entire bandwidth. Even though 100 kHz is more than sufficient for almost any imaginable experiment, we decided to test the limit and optimize a pulse for an even larger bandwidth by narrowing the compensation for RF inhomogeneity. An additional pulse, BIP–1382–300–10, was optimized for a ±60-kHz offset. The profile, not shown, also features nearly perfect inversion across the entire offset range. It should be noted that these pulses deviate from the adiabatic condition in that **M** does not follow the trajectory of the effective field at all times. In fact, the effective field both leads and lags on occasion, much like a whip does when cracked. These pulses do not require the adiabatic

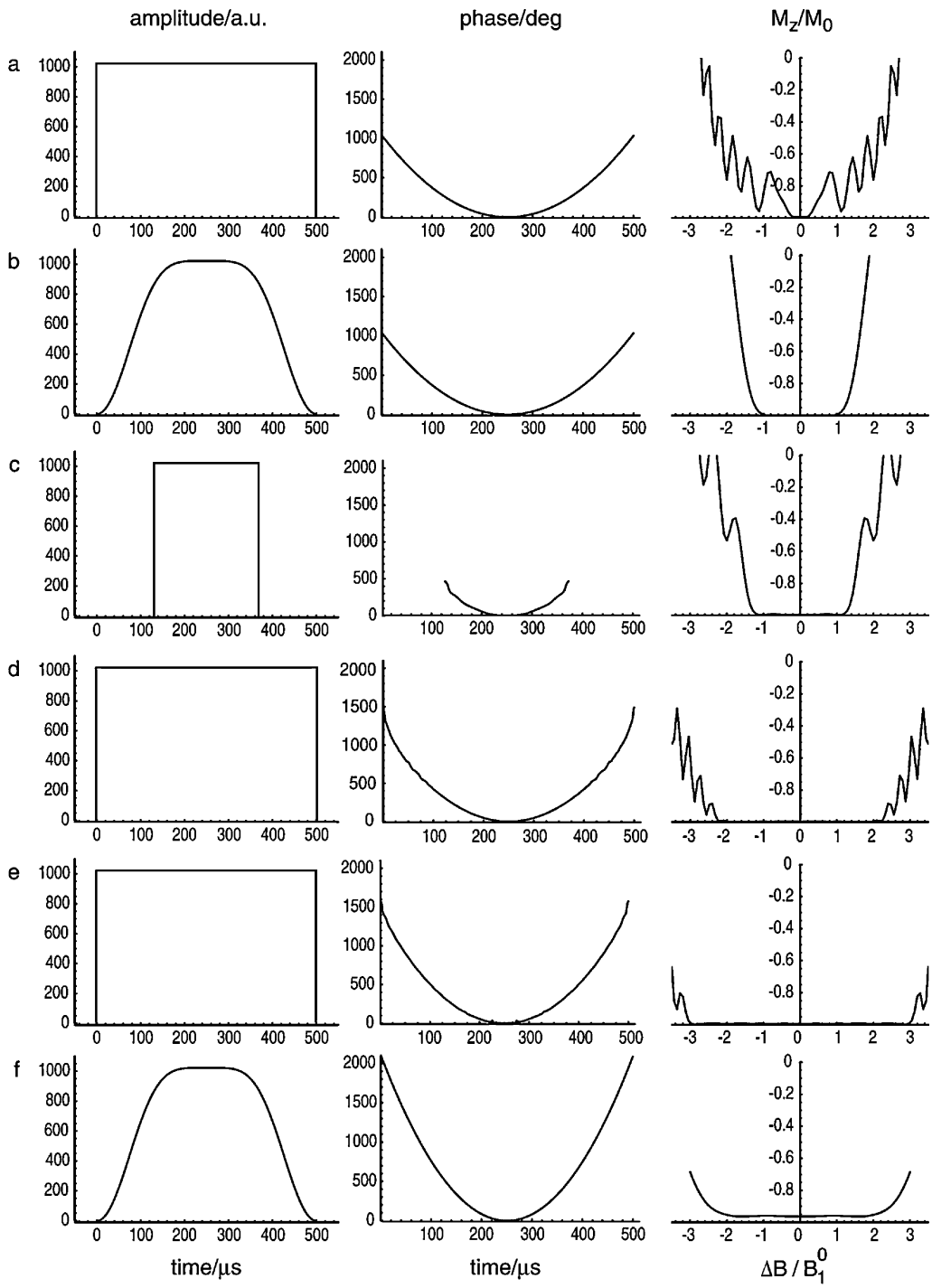

FIG. 7. A detailed comparison of 500-μs WURST-5 pulses and BIP pulses at a nominal field of 8.56 kHz, the conditions used in Ref. (9). The amplitude and phase functions are plotted on the left and center, and the inversion performance as a function of offset on the right. (a) A constant amplitude linear frequency sweep at 92 MHz/s. A limited inversion bandwidth is achieved, with oscillations in the performance. (b) A WURST-5 amplitude profile, and the same linear sweep as in (a) produces much better inversion performance, inverting well to $\Delta B/B_1^0 = \pm 1.2$. The adiabaticity on resonance is 5.0. (c) A constant-amplitude BIP of only 250 μs, showing inversion that is comparable to the WURST-5 pulse. The associated frequency sweep is nonlinear. (d) A BIP pulse using the full 500-μs time, showing superb inversion to $\Delta B/B_1^0 = \pm 2.0$. (e) A BIP inverting to $\Delta B/B_1^0 = \pm 3.0$. (f) A faster linear frequency sweep, corresponding to lower adiabaticity, allows the WURST-5 pulse to perform over a larger bandwidth than in (a), but cannot match the performance offered by the BIPs. Inversion begins to fail on resonance, much as the sech/tanh pulses with a larger R value, before the whole offset range is covered.

condition to be strictly met, and apparently this allows larger bandwidths to be obtained. We will illustrate this phenomenon with trajectories (*vide infra*).

The WURST pulses of Kupče and Freeman (*9, 10*) are another family of adiabatic pulses, and have been shown to invert larger bandwidths than the sech/tanh pulses under the constraints of identical T_p, B_1^{max}, and adiabaticity on resonance (Q_0) at least for the particular choice $Q_0 = 5$ (*9*). The WURST pulses have a purely linear frequency sweep and an empirically derived amplitude function of the form

$$B_1(t) = B_1^{max}\left(1 - \left|\sin\left(\frac{\pi t}{T_p}\right)\right|^n\right) \qquad [18]$$

with the adjustable positive integer n controlling the attenuation of the amplitude shape at the ends of the pulse. For relatively shorter pulses, ~1000°, n is typically smaller, in the region 2–10, becoming larger for longer pulses. In effect there is a relatively constant time relegated to the roll-off in amplitude, explaining this trend in the exponent n. The roll-off of the amplitude is necessary to guarantee that the effective field begins and ends parallel to the z axis, in an analogous fashion to the tangential sweep of the MIP pulses. To compare our BIPs with the WURST family, we adopt identical conditions to the shortest pulse in Ref. (*9*), namely a $T_p = 500\,\mu$s pulse with $\gamma B_1^{max}/2\pi = 8.56$ kHz, which is a pulse of length ~1540° in our notation. As we have no reason to believe that neither the BIP nor WURST pulse does not perform exactly as calculated, we employ simulation to contrast the two.

Figure 7 shows a comparison between a number of 500-μs inversion pulses. The phase and amplitude functions are shown in the left panels, with the inversion performance as a function of offset on the right. The first row is a constant-amplitude linear sweep at 92 MHz/s, showing very nonuniform inversion. The WURST-5 pulse, recommended in (*9*) with $n = 5$ and $Q_0 = 5$, is shown in the second row. The sweep rate is again 92 MHz/s. A bandwidth $\Delta B/B_1^0$ of about ± 1.2 is obtained, with very uniform performance over this range. Clearly, this seems to vindicate arguments based on adiabaticity. However, the third row shows that it is possible to obtain nearly the same performance as the WURST-5 pulse with a constant-amplitude nonlinear sweep that is only half as long! To illustrate that this pulse is not anomalous somehow, optimization of a full-length 500-μs BIP–1540–200–15 is shown in the fourth row. This pulse achieves essentially perfect inversion over the range $\Delta B/B_1^0 = \pm 2.0$. Finally, by altering the offset range and reoptimizing the waveform, the 500-μs BIP–1540–300–10 pulse, which covers $\Delta B/B_1^0 = \pm 3.0$, emerges in the fifth row. The final row shows an attempt to resurrect WURST-5 by increasing the sweep rate. The inversion over the bandwidth fails well before the offset range achievable by the BIP pulses is reached. Thus, just as WURST-5 trumps the equivalent sech/tanh pulse by leaving the B_1 field at the maximum level for longer, so the BIP pulse is better than WURST. As the pulse gets shorter and shorter, the linear frequency sweep method begins to fail altogether, no matter what value of the exponent n or adiabaticity Q is selected. The correct phase modulation for a short pulse is simply not a purely quadratic function, as demonstrated in Eq. [10] and Fig. 3. We

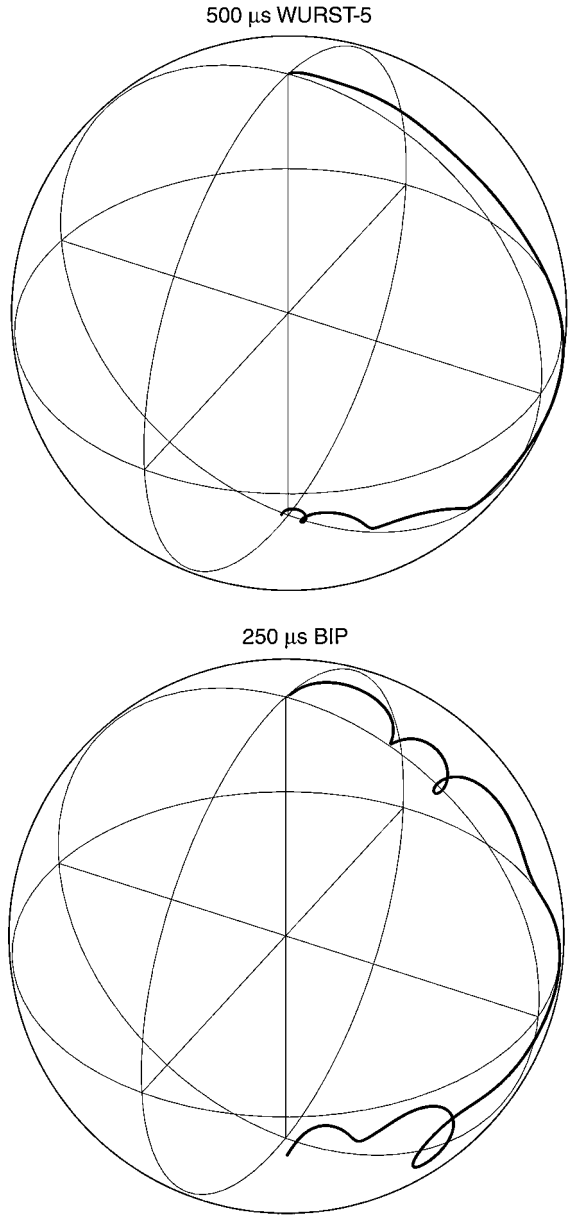

FIG. 8. Magnetization trajectories in the FM frame (*7*) in which adiabaticity is easier to visually gauge. The top trajectory is the 500-μs WURST-5 pulse of Fig. 7b, and corresponds to magnetization at the center of the inversion band (on resonance in the conventional rotating frame). The effective field is in the xz plane throughout, and the magnetization stays fairly close to it, lagging a little and showing some minor oscillations after the sweep has passed through resonance. The bottom trajectory is the BIP of only 250 μs shown in Fig. 7c. Because the field is turned on suddenly, the magnetization pitches toward the y-axis initially, and then plays catch-up in a cycloid-like fashion. The arabesques persist in the southern hemisphere, but nevertheless terminate with the magnetization quite near the south pole.

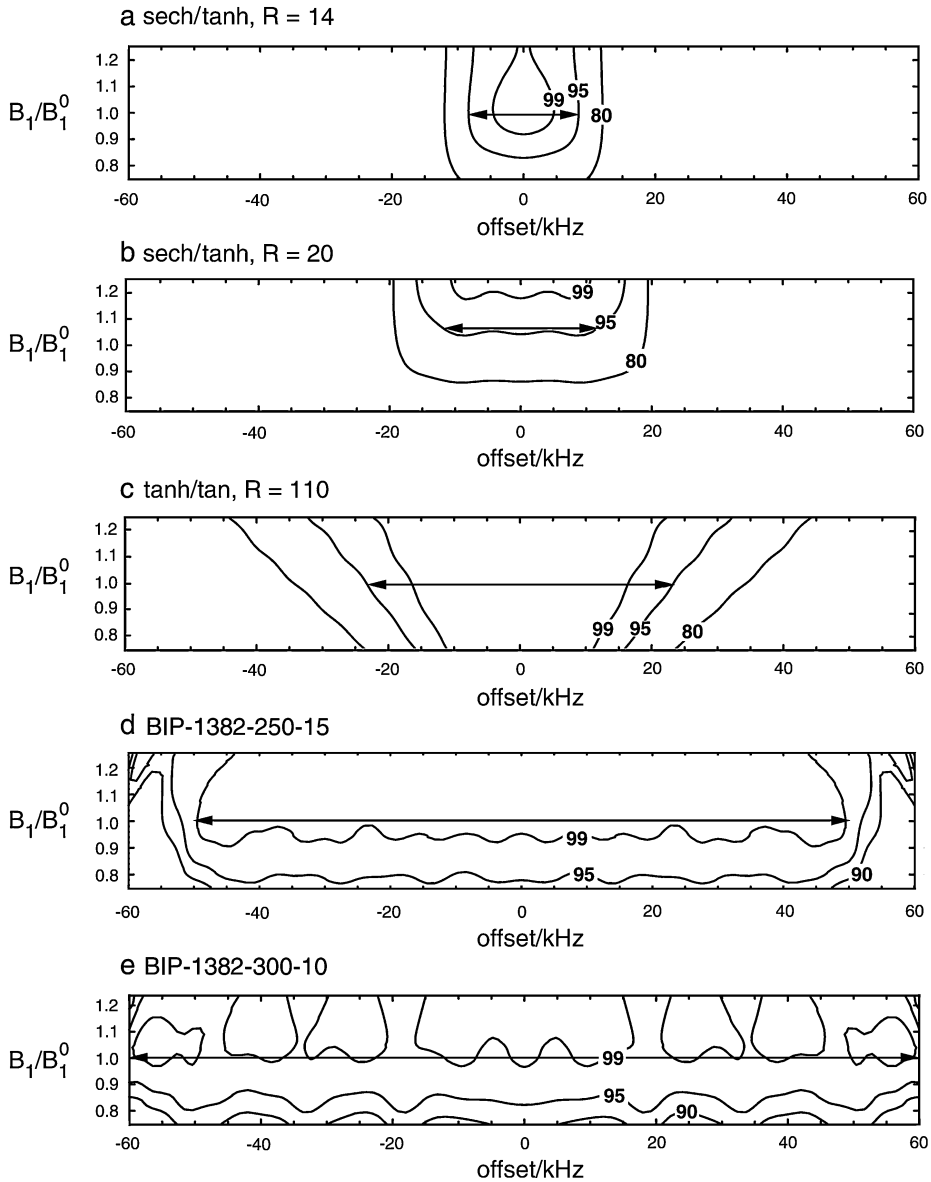

FIG. 9. Contour plots showing the inversion performance as a function of normalized resonance offset, $\Delta B/B_1^0$, and normalized RF field B_1/B_1^0. Contours are marked with the percentage inversion, with the horizontal double-headed arrows giving an indication of the usable bandwidth. The plots correspond to the experimental results of Fig. 6, except for the last plot. (a) A sech/tanh pulse, truncated at 1%, with $R = 14$. (b) A sech/tanh pulse, as in (a), but with $R = 20$. In agreement with the experiments, the entire map has shifted to higher B_1/B_1^0, so that inversion at the nominal field is incomplete on resonance. (c) The tanh/tan pulse (*12*) described in the text. The inversion bandwidth is superior to the sech/tanh pulses, but the region of good performance is not rectangular; i.e., the compensation for inhomogeneity varies with resonance offset. (d) Inversion performance of BIP–1382–250–15. (e) Inversion performance of BIP–1382–300–10. This offset bandwidth is the apparent limit for pulses of this length (1382°). Beyond this, inversion begins to fail noticeably nearer to resonance.

must emphasize that our design goal here is *not* long pulses nor those that are applied repetitively for broadband decoupling, for which the root-mean-square field, B_1^{rms}, is more relevant than B_1^{max}. Accordingly, we did not try to generate BIPs to compare with longer WURST inversion pulses described in (*9*).

Figure 8 shows two on-resonance magnetization trajectories, cast in the FM frame (*7*), and serves to contrast the WURST and BIP pulses. The top trajectory is that of the 500-μs WURST-5 pulse, whose offset dependence is shown in 7b. In the FM frame the effective field stays in the *xz* plane, and the magnetization trajectory for the WURST-5 also remains fairly close to this plane, and shows a smooth behavior throughout except for some minor oscillations toward the end. The 250-μs BIP pulse (see Fig. 7c) shows different behavior. The trajectory immediately swings away from the *xz* plane when the RF is suddenly switched on, and then plays leapfrog with the field as the trajectory continues. It nevertheless terminates quite near the south pole of the unit sphere.

Compensation for Pulse Miscalibration or RF Inhomogeneity

Rather than repeat the offset performance experiments with different B_1, it is more economical to show calculated contour plots of the expected performance of some BIPs. These are shown in Fig. 9, and agree quantitatively with experiment. The numerically optimized BIPs that push the offset performance envelope show inversion that is not numerically perfect to many digits (like the adiabatic pulses) near resonance, but that is nevertheless good enough for almost any experiment. The roughly rectangular areas over which good inversion is achieved show that the BIPs deliver inhomogeneity compensation that is independent of resonance offset. The adiabatic pulses show the typical skewing of better inversion at stronger B_1 fields, and smaller bandwidths with respect to resonance offset. When comparing to adiabatic pulses, it is therefore important to be very strict in the specification of $B_1^{\max}$. It is always possible to run an adiabatic pulse a little bit "hot" (+1 or +2 dB) compared to "nominal" to compensate for weaker RF regions over the sample volume. Our claim is that a correctly calibrated BIP will be shorter and better than even a "slightly hot" adiabatic pulse.

CONCLUSIONS

The correct amplitude modulation envelope for a short pulse under the constraints of fixed peak RF field and fixed duration is a constant amplitude at the maximum available field $B_1^{\max}$. The resulting inversion pulse, which we designate a *b*roadband *i*nversion *p*ulse (BIP), is ideal for most NMR experiments in liquids. The correct frequency sweep is *not* a tangential sweep (*4, 7*), as evidenced by the results of this study. BIPs have associated frequency sweeps that are definitely nonlinear, but not identifiable as any other simple functional form either. BIPs can be employed in lieu of conventional 180° pulses in common pulse sequences, with only slight modification of the pulse sequence. They are convenient to use, relatively short in duration, and work well in practice. As no amplitude modulation is used, linearity of the RF amplifier is unimportant. For cases in which the offset range is not enormous, short and highly effective inversion pulses, of similar spirit to the early composite pulses, can be employed. When the offset range *is* enormous the BIPs tend toward adiabatic pulses, but seem to maintain an edge in performance by allowing nonadiabatic trajectories which just happen to invert well. Indeed, so-called offset-independent adiabaticity (*10*), in which the sweep is chosen so as to maintain similar adiabaticity for all offsets in the operating band, proved to slightly degrade the inversion bandwidth of a WURST-20 pulse rather than enhancing it. It is thus not too surprising that deliberately ignoring adiabaticity, especially at the edges of the working bandwidth, might have the opposite effect.

The BIPs can be used in a wide variety of ways. For inversion and single-pulse heteronuclear decoupling applications, BIPs may be substituted for conventional 180° pulses. For spin echo applications, BIPs should be used in pairs to cancel out unwanted phase shifts over the working bandwidth, a feature noted in the earliest composite pulse spin echo work (*23*) and rediscovered for adiabatic pulses (*24*) later. A simple way to operate is to replace a $90°–\tau–180°–\tau$ spin echo sequence with a $90°–180°–\tau–180°–\tau$ sequence, where the role of the initial 180° is simply to correct the phase roll produced by the second. For other applications see Refs. (*20*) and (*21*).

The term "adiabatic" has been synonymous with "efficient and broadband" in the minds of many, especially where inversion pulses are concerned. This work shows that adiabatic pulses, rather than being the most efficient, may actually waste precious time so that the adiabatic condition can be fulfilled. When a short high-power pulse is desired, BIPs are superior. While BIPs seem like the best pulse shape(s) under the constraints of given $B_1^{\max}$ and duration, they show no particular or predictable performance outside the bandwidth, much like composite pulses. They are thus not particularly useful for selective pulse applications. It may be possible to include the amplitude as a variable as well, to generate selective, partially selective, or nonselective pulses with different constraints. These pulses would be of interest in decoupling applications, for example. A preliminary foray into this area has already shown that constant-amplitude pulses are not optimum when B_1^{rms} is the relevant constraint (*25*). We will report on these developments in future publications.

ACKNOWLEDGMENT

This work was supported by the National Science Foundation, NSF CHE-9900422.

REFERENCES

1. M. H. Levitt and R. Freeman, NMR population inversion using a composite pulse, *J. Magn. Reson.* **33,** 473–476 (1979).
2. A. J. Shaka, J. Keeler, T. Frenkiel, and R. Freeman, An improved sequence for broadband decoupling: WALTZ-16, *J. Magn. Reson.* **52,** 335–338 (1983).
3. A. J. Shaka, J. Keeler, and R. Freeman, Evaluation of a new broadband decoupling sequence: WALTZ-16, *J. Magn. Reson.* **53,** 313–340 (1983).
4. J. Baum, R. Tycko, and A. Pines, Broadband population inversion by phase modulated pulses, *J. Chem. Phys.* **79,** 4643–4644 (1983).
5. M. H. Levitt and R. R. Ernst, Composite pulses constructed by a recursive expansion procedure, *J. Magn. Reson.* **55,** 247–254 (1983).
6. M. S. Silver, R. I. Joseph, and D. I. Hoult, Selective spin inversion in nuclear magnetic resonance and coherence optics through an exact solution of the Bloch-Riccati equation, *Phys. Rev. A.* **31,** 2753–2755 (1985).
7. J. Baum, R. Tycko, and A. Pines, Broadband and adiabatic inversion of a two-level system by phase-modulated pulses, *Phys. Revs. A* **32,** 3435–3446 (1985).
8. A. J. Shaka, Composite pulses for ultra-broadband spin inversion, *Chem. Phys. Lett.* **120,** 201–205 (1985).

9. E. Kupče and R. Freeman, Adiabatic pulses for wideband inversion and broadband decoupling, *J. Magn. Reson. A* **115,** 273–276 (1995).
10. E. Kupče and R. Freeman, Optimized adiabatic pulses for wideband spin inversion, *J. Magn. Reson. A* **118,** 299–303 (1996).
11. A. Tannus and M. Garwood, Improved performance of frequency-swept pulses using offset-independent adiabaticity, *J. Magn. Reson. A* **120,** 133–137 (1996).
12. T. Hwang, P. van Zijl, and M. Garwood, Fast broadband inversion by adiabatic pulses, *J. Magn. Reson.* **133,** 200–203 (1998).
13. J. Briand and R. R. Ernst, Computer-optimized homonuclear TOCSY experiments with suppression of cross relaxation, *Chem. Phys. Lett.* **185,** 276–285 (1991).
14. N. Metropolis, A. W. Rosenbluth, M. N. Rosenbluth, A. H. Teller, and E. Teller, Equation of state calculations by fast computing machines, *J. Chem. Phys.* **21,** 1087–1092 (1953).
15. H. Geen and R. Freeman, Band-selective radiofrequency pulses, *J. Magn. Reson.* **93,** 93–141 (1991).
16. H. Geen, S. Wimperis, and R. Freeman, Band-selective pulses without phase distortion. A simulated annealing approach, *J. Magn. Reson.* **85,** 620–627 (1989).
17. A. Abragam, "The Principles of Nuclear Magnetism," Oxford Univ. Press, Oxford (1961).
18. J. S. Waugh, Systematic procedure for constructing broadband decoupling sequences, *J. Magn. Reson.* **49,** 517–521 (1982).
19. A. J. Shaka and R. Freeman, Composite pulses with dual compensation, *J. Magn. Reson.* **55,** 487–493 (1983).
20. V. A. Mandelshtam, H. Hu, and A. J. Shaka, Two-dimensional HSQC NMR spectra obtained using a self-compensating double pulsed field gradient and processed using the filter diagonalization method, *Magn. Reson. Chem.* **36,** S17–S28 (1998).
21. H. Hu and A. J. Shaka, Composite pulsed field gradients with refocused chemical shifts and short recovery time, *J. Magn. Reson.* **136,** 54–62 (1983).
22. T. Hwang, M. Garwood, A. Tannus, and P. van Zijl, Reduction of sideband intensities in adiabatic decoupling using modulation generated through adiabatic R-variation (MGAR), *J. Magn. Reson. A* **121,** 221–226 (1996).
23. M. H. Levitt and R. Freeman, Compensation for pulse imperfections in NMR spin-echo experiments, *J. Magn. Reson.* **43,** 65–80 (1980).
24. S. Conolly, G. Glover, D. Nishimura, and A. Macovski, A reduced power selective adiabatic spin-echo pulse sequence, *Magn. Reson. Med.* **18,** 28–38 (1991).
25. P. B. Barker, X. Golay, D. Artemov, R. Ouwerkerk, M. A. Smith, and A. J. Shaka, Broadband proton decoupling for *in vivo* brain spectroscopy in humans, *Magn. Reson. Med.* **45,** 226–232 (2001).